



Study on the response of postside-grouted piles subjected to lateral loading in calcareous sand

Zhi-hui Wan¹ · Guo-liang Dai² · Wei-ming Gong²

Received: 25 February 2021 / Accepted: 10 October 2021 / Published online: 1 November 2021
© The Author(s), under exclusive licence to Springer-Verlag GmbH Germany, part of Springer Nature 2021

Abstract

The post-grouting technique has gradually become an effective approach to improve the bearing capacity of piles in calcareous sand due to its simple process, low cost and reliable reinforcement effect. In this paper, model tests were performed on horizontally loaded single piles under static pressure pile driving in a calcareous sand foundation. The responses of ungrouted piles and post-grouted piles subjected to lateral loads in calcareous sand were studied, the test results were compared with those of ungrouted piles and post-grouted piles in siliceous sand, and the influence of postside grouting on the horizontal bearing behavior of piles in calcareous sand was explored. The results show that due to the particularity of the calcareous sand, its horizontal restraint ability of ungrouted piles is weaker than that in siliceous sand. Post-grouting at the pile side has a significant effect on improving the horizontal bearing capacity and strengthening the deformation control ability of the pile in calcareous sand, while showing approximately the same characteristics as that of the post-grouted pile in siliceous sand under the same conditions. The ratio of the lateral resistance coefficient of ungrouted and post-grouted piles gradually tends to be consistent with the increase in the lateral displacement of the pile head, and the bending moment and lateral displacement of the pile shaft are mainly concentrated in the upper part of the pile shaft. The lateral bearing capacity of the pile is greatly affected by the upper level of soil, and grouting at the pile side can effectively increase the ability of the pile foundation to resist horizontal loads and control deformation by improving the physico-mechanical properties of the upper soil layer. In addition, the distribution and microstructure of cement-stabilized soil are analyzed based on the excavation of a post-grouting single pile. It is found that the cement grout injected at the pile side moves upward, penetrates downward and diffuses horizontally along the pile shaft to form a stable structure of cement-stabilized soil with calcareous sand particles; therefore, the pile–soil system interaction enters a new structural equilibrium state, thereby improving the horizontal bearing capacity of the pile foundation in calcareous sand.

Keywords Calcareous sand · Cement-stabilized soil · Lateral bearing capacity · Microstructure · Model test · Postside-grouted pile

1 Introduction

With the continuous emergence of large-span and large-scale buildings or structures in the construction of coral reefs, the method of reclaiming land on extremely shallow

reefs is no longer suitable for deeper reefs, sands or shoals. Pile foundations are widely used in engineering construction projects because of their high bearing capacity, good stability and uniform settlement. The combination of pile foundations and hydraulic fill islands can effectively serve the construction of island and reef infrastructures. At present, pile foundations have been widely used in high compressibility foundations such as those in calcareous sand [2, 3, 11, 13, 32, 37]. However, due to the unique physical and mechanical properties of calcareous sand, such as high porosity, easy cementation and easy breakage, construction disturbance easily causes particle breakage and stress relaxation of the calcareous sand around the pile,

✉ Guo-liang Dai
daigl@seu.edu.cn; seudaigl@126.com

¹ School of Transportation Engineering, Nanjing Tech University, Nanjing 211816, China

² Key Laboratory of Concrete and Prestressed Concrete Structures of Ministry of Education, School of Civil Engineering, Southeast University, Nanjing 211189, China

resulting in weakening of the side friction and tip resistance, thus reducing the bearing capacity of the pile foundation [1–3, 10, 17, 18]. This also causes the traditional design and analysis methods of the bearing capacity of pile foundations for terrigenous sediments to be inadequate for calcareous sediment; therefore, the performance of pile foundations in calcareous sand has become very concerning problem in engineering applications and academia.

The post-grouting technique has become the method used by engineering and academic groups to improve the bearing capacity of pile foundations in calcareous sand due to its simple process, low cost and reliable reinforcement effect. At present, the post-grouting technique can be divided into three categories: post-grouting at the pile tip, post-grouting at the pile side and combined post-grouting at the pile tip and side. Wan et al. [34] summarized the post-grouting apparatus at the pile tip and pile side in detail. Post-grouting at the pile tip was first applied in engineering practice in 1958, and subsequently, it has been widely applied and developed all over the world. A large number of research results have been achieved on the influence of post-grouting at pile tip on the bearing mechanism and mechanical behavior of pile [4, 8, 20, 30, 34, 35]. Compared with post-grouting at pile tip, post-grouting at pile side started slightly later. Postside grouting can effectively improve the boundary conditions between the pile side and soil and enhance the shaft resistance, thus greatly improving the horizontal and pull-out forces. Therefore, postside grouting has been gradually applied to large-scale bridges, high-speed railways, high-rise tower buildings, port terminals and offshore oil platforms [5, 14, 16]. Theoretical research and practical applications of combined post-grouting at both the pile tip and side are more complicated than those of post-grouting at the pile tip or side alone, which has led to fewer research reports on combined tip-and-side grouting. Robson and Wahby [23] reported that the shaft resistance of a cast-in-place pile after combined tip-and-side grouting in a sandy soil area in Egypt increased by 2 to 3 times compared with that of an ungrouted pile. Thiyyakkandi et al. [29] designed a grouting device for use at the pile tip and side of a pre-fabricated pile and conducted model pile tests using this device. The results showed that good bonding between the pile and cement grout promoted the development of the shaft and tip resistances. Wan et al. [32, 34, 35] studied the bearing deformation performance, load transfer law and design method of combined tip-and-side pile-grouting based on field static load test results, and the results can provide a reference for the economical and reasonable application of combined post-grouting in engineering practice. In addition, Zhou et al. [38–40] presented a pre-bored grouted planted pile, and the friction performance of

pile–soil interface and compressive bearing behavior of pre-bored grouted planted pile were investigated by shear tests and field static load tests.

The execution of many important projects, such as the National Stadium of the Bahamas, the Port of Saudi Arabia, and the Male-Airport Island Cross-sea Bridge in the Maldives, has shown that post-grouted pile foundations can satisfactorily meet the functional and safety requirements of coral reef projects in serviceability limit states. Ghazali et al. [12] introduced the construction process of large-diameter post-grouted piles on the coral reef in the Red Sea and the basis for the selection of pile types in this area and presented the static load test results of three on-site post-grouted piles. This shows that the post-grouting technique applied to bored piles in this formation can meet the requirements of foundation design. Joer et al. [15] performed tests by driving multiple groups of side grouting into piles in calcareous sand through the developed side grouting model device and studied the estimation of the ultimate bearing capacity and the relationship between the grout coverage and grouting pressure. Chen [6] used advanced drilling and grouting to treat a coral reef pile foundation in the Bahamas, and the bearing capacity of the pile foundation met the design requirements after grouting. Wan et al. [31, 33] performed a static load test on post-grouted piles in coral reefs and compared and analyzed the measured results before and after grouting. It was found that the post-grouting technique can be applied to coral reef strata and can effectively improve the bearing capacity of pile foundations. In addition, some scholars have proposed method to drilled and grouted piles to improve the bearing capacity of pile foundations in calcareous sand that cannot meet the engineering requirements [21, 37]. The main construction process is as follows: the steel casing is pre-driven before drilling, the mechanical equipment is drilled to the predetermined position, and then the steel pipe pile is inserted into the bottom of the hole. Finally, the whole construction process is completed by grouting inside and outside at the pile tip. In this method, the hole diameter is larger than the outer diameter of the pile, and the grout is poured into the pile where it fills the outer gap of the pile and bond the soil around the pile. This method is obviously different from the post-grouting method, and the large amount of grout required can easily cause shrinkage after consolidation, which is disadvantageous to the improvement of the bearing capacity of the pile foundation.

However, the existing findings mostly focus on the response of post-tip grouted piles subjected to vertical loads in calcareous sand, and there are few studies on the response of postside-grouted piles in calcareous sand. In practical engineering applications, calcareous sand pile foundations are subjected to more frequent horizontal loads in large projects, such as those involving cross-sea bridges,

port terminals, offshore oil platforms and offshore wind turbines. However, there are few reports on the influence of post-grouting on the response of piles subjected to lateral loading in calcareous sand. Therefore, it is of practical significance and application value to study the horizontal bearing behavior of post-grouted piles in calcareous sand under horizontal external forces.

In this paper, a simple self-designed static pressure device is used to perform horizontal loading tests on steel pipe piles based the static pressure pile driving method in a model foundation of calcareous sand, and the response of a single pile subjected to lateral loading in calcareous sand is studied. On this basis, a comparative study of ungrouted piles and post-grouted piles in calcareous sand was performed, and the test results were compared with those of ungrouted piles and post-grouted piles in siliceous sand to explore the effect of post-grouting on the response of piles subjected to lateral loading in calcareous sand.

2 Small-scale experiments

2.1 Model preparation

Steel pipe piles are widely used in offshore engineering. Combined with its practical application in offshore platforms, this model test analyzes large-diameter steel pipe piles with a diameter of 1.2 m in the field. Based on the principle of similarity theory, the geometric model similarity constant ($C_L = L_p/L_m$) is 60:1, and the elastic modulus similarity constant ($C_E = E_p/E_m$) is 1:1 for the selected model test, where L_p and L_m are the dimensions of the prototype and model, respectively, and E_p and E_m are the elastic modulus of the prototype and model, respectively. Hence, this model pile adopts a small-scale steel pipe pile with an outer diameter of 20 mm, wall thickness of 1 mm, and length of 500 mm. To protect the strain gauge from being affected during the test, it is adhered on the inner wall of the model pile, so the steel pipe pile must be cut in half along the longitudinal direction. The wire of the strain gauge is drawn from the hole of the pile shaft, and a seamless steel pipe is formed by the spot welding method. In addition, the bottom of the pile is welded with a steel sheet of suitable size and the same type of material as the pile, and the thickness of the steel sheet is 2 mm. The fabricated model piles are shown in Fig. 1.

The size of the model container should meet the requirements of the distance between the model pile and its inner wall and end and the condition that the filling medium is a semi-infinite body. In this test, a square iron model container with a length and width of 36 cm and height of 70 cm was adopted, and its wall thickness was 15 mm. Oveson [22] proposed that the distance between the model

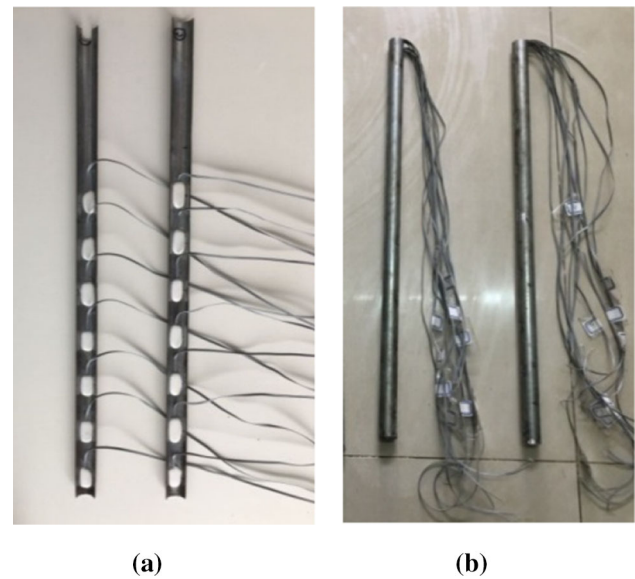


Fig. 1 Model pile: **a** profile view and **b** assembly drawing

and the inner wall of the container should be greater than 2.82 times the size of the model, which can eliminate the influence of the boundary effect on the test results. The selection and arrangement of the model piles in this test conform to the boundary effect caused by the inner wall of the model container. The later model test indicated that the model container can bear a sufficiently large load and meet the requirements of this test.

The calcareous sand used in this experiment was uncemented loose coral debris deposits from the South China Sea. To illustrate the influence of postside grouting on the bearing behavior of piles in calcareous sand, siliceous sand was also used for a comparison of the model foundation material. To produce similarly the particle size curves for the two kinds of sand samples, the model foundation materials were provided by controlling the parameters such as the particle size distribution, moisture content and density of the sand samples. The particle size distribution was used as the main control index, and the moisture content and density were used as the auxiliary reference values. Craig [7] pointed out that a model structure larger than 40 times the particle size would not affect the bearing capacity of the foundation. The particle size selected in this experiment was less than 1 mm, which could avoid the influence of the particle size of the model foundation material on the bearing behavior of a single pile. The sand samples were screened to obtain sand samples with different particle sizes. According to the screening test results and the percentage of particle size mass in each range, the uniformity coefficient C_u and curvature coefficient C_c of the two sand samples were obtained as 3.34 and 1.19, respectively. The particle size distributions of the two kinds of sand samples are shown in Fig. 2.

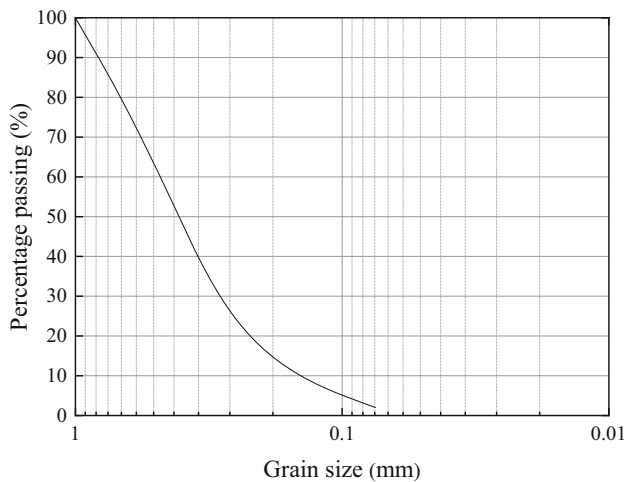


Fig. 2 Particle size distribution

Because calcareous sand is prone to particle breakage under cyclic vibration loads, the method of obtaining the maximum dry density through geotechnical tests is unreasonable, and it is difficult to obtain the relative compactness of calcareous sand. Therefore, in this test, the two sand samples are controlled by the paving layer thickness (10 cm per layer) and single-layer compaction times (50 times per layer). To allow the compactness of sand samples to better reflect that of the actual situation, backpressure was applied to the model foundation according to similarity theory and the deadweight stress of the sand samples, and the backpressure load was applied to the surface layer of sand at 100 kPa. Due to the small clay content of sand and fast consolidation settlement, the sand sample of the model foundation quickly became stable after the reverse pressure was applied, and then unloading was performed after reverse pressure was applied for 1 h. By measuring the parameters of the sand samples of the model foundation, it is evident that the physicochemical parameters of the two sand samples are relatively close, as shown in Table 1.

2.2 Pile driving test and grouting device

A simple self-designed static pressure device is used to realize the driving effect of steel pipe piles and simulate the

penetration process of steel pipe piles in practical engineering. After the reverse pressure load of the model foundation is removed, the model foundation is allowed to stand for no less than 12 h before the pile driving test is performed. First, the model of a single pile is set in the predetermined position, and the steel pressing plate is fixed in place through the threaded rod to complete the preparation before pile driving is performed. Second, torque is applied to the fastening nuts on both sides to cause the steel plate to penetrate the model pile into the sand sample of the model foundation. It is necessary to control the penetration speed to ensure that the model pile remains vertical during the process of pile driving. The penetration depth of the model pile is recorded every 2 min by a time recorder, and the verticality of the model pile is corrected by a horizontal ruler. Finally, the driving test of the model pile is completed according to the same method mentioned above.

To investigate the influence of postside grouting on the bearing behavior of steel pipe piles in calcareous sand, two grouting pipes with a diameter of 8 mm are placed in the model pile for the postside-grouting tests. The bottom of the grouting pipe is 22.5 cm away from the pile head and is connected to the inner wall of the pile. The size of the grouting hole is 8 mm, and the holes are sealed with pushpins. The specific post-grouting pipeline at the pile side is arranged as shown in Fig. 3. The postside-grouting test is performed by a self-developed grouting device. The post-grouting device is mainly composed of an oil pump, hydraulic oil actuator, grout tank, working platform and grouting valve, as shown in Fig. 3. Before the postside-grouting test is performed, the grouting device is used to inject water into the grouting pipe to break the pushpins on the grouting hole and to ensure the smooth flow of the pipeline system. Before grouting is implemented, the prepared cement grout must be absorbed through the grouting device, where it is stored in a grout tank with a storage capacity of 1.05 L. A three-way joint is used to connect the grouting pipe to the grouting pipe in the model pile, and the oil pump is adjusted to control the grouting pressure and grouting rate so that the injected grout enters the sand sample of the model foundation through the grouting hole, and the post-grouting test at the pile side is completed. In

Table 1 Physicochemical parameters of the sand foundations

Sand type	Density, ρ ($\text{g}\cdot\text{cm}^{-3}$)	Moisture content, ω (%)	Void ratio, e	Relative density, d_s	Internal friction angle, φ ($^\circ$)	Compression modulus, E_{s1-2} (MPa)
Calcareous sand	1.56	22.05	0.97	2.52	36.38	15.39
Siliceous sand	1.68	19.78	0.84	2.58	32.31	25.13

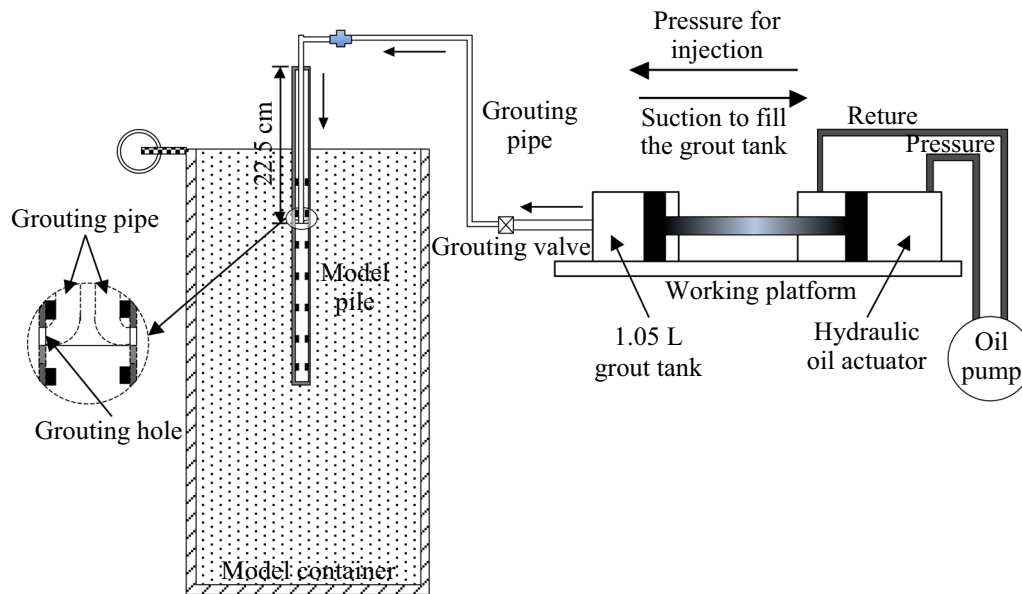


Fig. 3 Post-grouted apparatus

this experiment, static load tests are performed on four model piles, including ungrouted pile MP1 and grouted pile MP2 in calcareous sand and ungrouted pile MP3 and grouted pile MP4 in siliceous sand performed.

2.3 Test set-up, test method and instrumentation

For piles without grouting, the horizontal static load test is performed 24 h after the pile driving is complete. For grouted piles, the grouting test is performed immediately after pile driving, and the horizontal static load test is performed 28 days after the completion of grouting. In the static load test, the slow maintenance load method was used to obtain the ultimate bearing capacity of the ungrouted and grouted piles in the horizontal direction according to the pretest. The ultimate bearing capacity of the ungrouted and grouted piles in the horizontal direction was incrementally loaded at 1/10 of the estimated maximum test load, and the magnitude of the first load step was double that of the subsequent load steps. The unloading decrements were twice the loading increments during the unloading test. Based on the Chinese standard (JGJ 106–2014) [26], the pile head lateral displacement of a single pile under this level of load was not more than 0.1 mm per hour for two consecutive times, then the next level of load could be applied, and the maintenance time of each level of load was not less than 1 h. The condition of test termination was that when the horizontal displacement of a single pile was too large to continue to increase the load, the horizontal displacement of a single pile increased sharply when loaded, or the deformation rate accelerated

significantly. The horizontal static load test of a single pile is shown in Fig. 4.

Strain gauges are arranged symmetrically along the inner surface of the steel pipe to study the bearing characteristics of steel pipe piles in calcareous sand. According to the actual penetration depth of the model pile, the pile is divided into seven sections from top to bottom, and each section is symmetrically arranged with two strain gauges to measure the strain of the corresponding section of the pile shaft. The specific arrangement is shown in Fig. 4. During the whole loading process, the strain gauge data are collected by the static strain testing system. The measurement of the pile head displacement is an important part of this test. The lateral displacement of the pile head is measured by a dial gauge with a range of 0–50 mm and an accuracy of 0.01 mm. Two dial gauges are directly installed on both sides of the model of a single pile and symmetrically maintained at the same horizontal level. The average of the results of the two dial gauges is used to obtain the lateral displacement of the model of a single-pile head. In addition, to measure the change in earth pressure in the sand sample of the model foundation, miniature fiber Bragg grating (FBG) earth pressure cells labeled F1 to F9 are embedded around the pile. The specific layout is shown in Fig. 4.

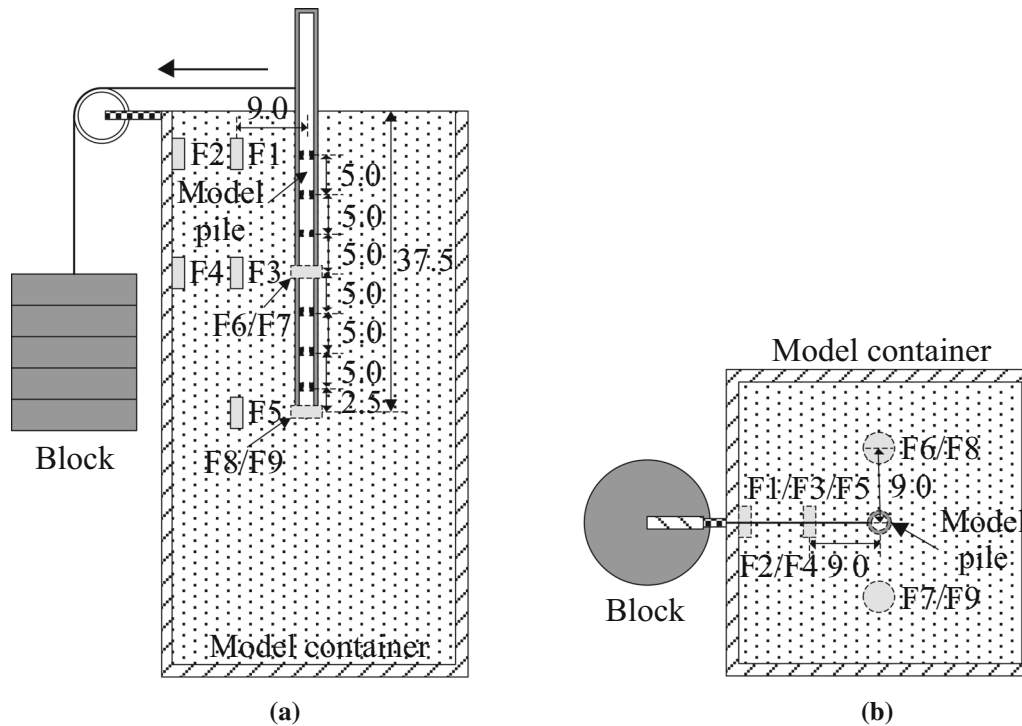


Fig. 4 Lateral static load test of a single pile and testing element arrangement (unit: cm): **a** front view and **b** vertical view

3 Experimental procedure and phenomenon analysis

3.1 Variation in earth pressure under reverse pressure loading

The purpose of this test is to perform a comparative analysis of the bearing characteristics of a single pile in calcareous sand and siliceous sand, and it is necessary to control the relative compactness of the two sand samples so that their values are as close as possible. On the one hand, the paving layer thickness and single-layer compaction pass methods are used to control the sand sample of the model foundation in this test; on the other hand, the reverse pressure load is applied to control the sand sample of the model foundation. Before the reverse pressure load is applied, the data obtained from the miniature FBG earth pressure cells before loading are collected by a portable FBG demodulator, and then the sample is unloaded after the entire reverse pressure load is applied for 1 h. The variation in earth pressure with time is monitored by the miniature earth pressure cell, and the earth pressure at 1, 3, 6 and 12 h after unloading is observed and recorded. The variation in earth pressure at each stage of backpressure loading and unloading is obtained, as shown in Fig. 5.

Figure 5 shows that the earth pressure increases linearly after the backpressure load is applied, and the change in earth pressure is not obvious after the backpressure load is

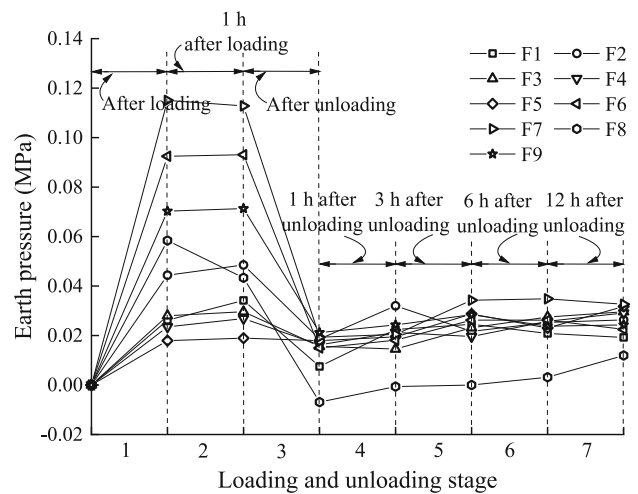


Fig. 5 Changes in earth pressure during loading and unloading

maintained for 1 h. However, the earth pressure decreases rapidly after unloading and gradually tends to a stable value with time. Therefore, the pile driving test can be performed approximately 12 h after unloading. This indicates that the consolidation of the sand samples of the model foundation is basically complete after 1 h under the reverse pressure load, and the earth pressure tends to a certain stable value 12 h after unloading due to the dissipation of pore water pressure and the increase in effective stress. Figure 5 also shows that the average value of the data for F6 and F7 of the miniature earth pressure cell is

0.1029 MPa after the reverse pressure load is applied for 1 h, and the value of F3 of the miniature earth pressure cell in the same plane is 0.0296 MPa, and then the static earth pressure coefficient K_0 can be obtained as 0.29. At the same time, the average value of the data for F8 and F9 of the miniature earth pressure cell is 0.0573 MPa after the reverse pressure load is applied for 1 h, and the value of F5 of the miniature earth pressure cell in the same plane is 0.019 MPa, and then the static earth pressure coefficient K_0 can be obtained as 0.33.

3.2 Analysis of the pile driving test results

Pile driving tests are performed with a simple static pressure device approximately 12 h after the reverse pressure load is removed from the model foundation. During the test, it is necessary to pay special attention to the speed of the steel plate when applying torque to control the speed of pile driving and ensure that the steel pipe pile remains perpendicular. In addition, the penetration depth of the steel pipe pile is measured and recorded every 2 min, which is the penetration period during the pile driving process, and the perpendicularity of the steel pipe pile is corrected with a horizontal ruler. Based on the requirements discussed above, the steel pipe pile penetrates into the specified position to complete the pile driving test. By sorting out the recorded data, the relationship between the penetration rate and penetration depth in the process of the single-pile driving test can be obtained, as shown in Fig. 6.

Figure 6 shows that in the initial stage of pile driving, due to the shallow depth of the steel pipe pile in the soil, the sand soil of the model foundation provides less resistance to pile driving than that with a less shallow depth,

resulting in a faster pile driving rate. In the subsequent process of pile driving, as the penetration depth of the steel pipe pile increases, the soil around the pile has a compaction effect due to the influence of pile driving, which increases the resistance of pile driving and leads to the decrease in the penetration rate of steel pipe pile with the increase in the penetration depth. Figure 6 also shows that the penetrations rates of the two steel pipe piles in calcareous sand are roughly the same as the penetration depth changes. At the same time, the penetration rates of the two steel pipe piles in siliceous sand are also basically the same as the penetration depth changes. This shows that the homemade simple pile driving device can simulate the penetration process of steel pipe piles in practical engineering by controlling the pile driving rate. In addition, by comparing the relationship between the penetration rate and penetration depth of the two sand samples, it is evident that the values of relative compactness of the two sand samples are close. This further indicates that controlling the paving layer thickness, single-layer compaction times, and reverse pressure load are simple and effective methods for controlling the relative compactness of the sand samples in this test.

3.3 Analysis of the post-grouting test

A postside-grouting test is performed to inject the water into the grouting pipe and break the pushpins on the grouting hole. The main function of the injected water test is to dredge the grouting pipe and ensure that the pipeline system is unblocked. The literature [9] shows that the water–cement ratio of post-grouted piles is mainly distributed in the range of 0.5 to 0.7 based on statistics; thus,

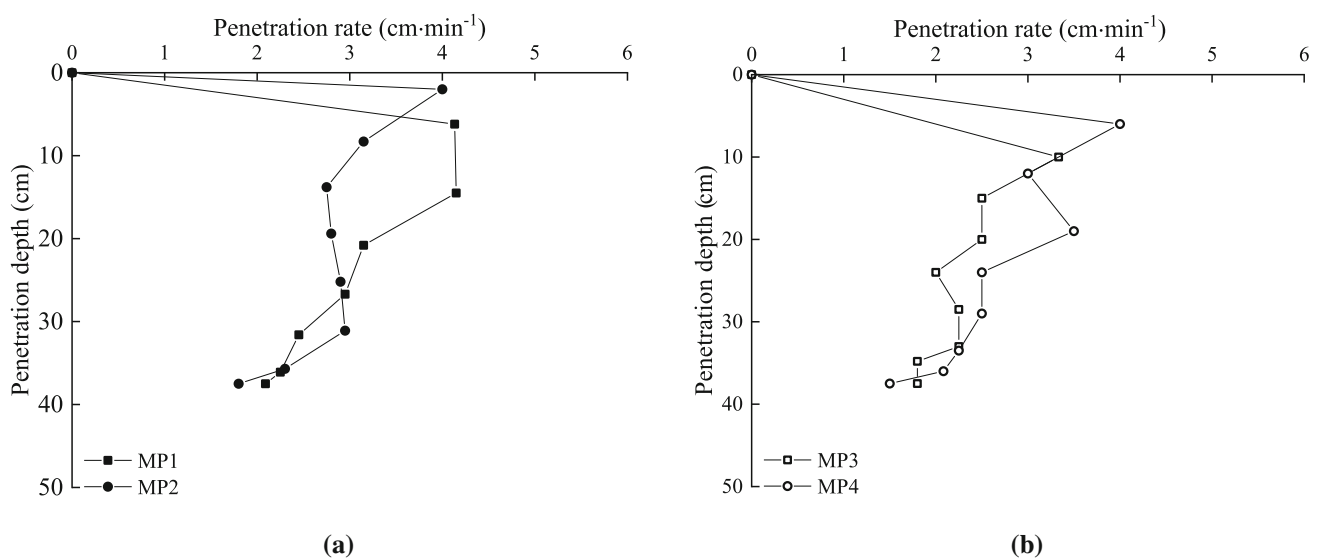


Fig. 6 Relationship between the penetration rate and penetration depth: **a** calcareous sand and **b** siliceous sand

the water–cement ratio prepared in this experiment is 0.6. The prepared cement grout is sucked into the grout tank through the grouting device and all the required preparations before grouting are completed. Then, the postside-grouting test is performed. The grouting pressure and grouting rate are controlled by adjusting the oil pump during the grouting process. Throughout the test process, the fluctuation range of the grouting pressure of the two sand samples is 0.25–0.3 MPa. When the grouting volume is approximately 200 mL, the sand surface of the two model foundations is uplifted, and the grouting test is terminated.

4 Results and analysis

4.1 Lateral load–displacement response of a single pile

The lateral load–displacement responses of ungrouted and grouted piles are shown in Fig. 7. Figure 7 shows that the lateral displacement of the pile head increases slowly when the load level is small, and the pile–soil system is in an elastic working state and does not produce plastic deformation at this stage. The lateral displacement of the pile head increases gradually with increasing lateral load of the pile head and increases rapidly when the load exceeds a certain value. The lateral load–displacement response of a single pile exhibits an obvious nonlinear relationship, indicating that the soil around the pile gradually enters a plastic state. The elastic stage of the lateral displacement changes when the lateral load of the pile head is very short, and ungrouted pile MP1 quickly enters the elastic–plastic

stage when it is subjected to lateral loading in calcareous sand. This is why the particle fragility of calcareous sand causes obvious elastic–plastic deformation when it is subjected to lateral loading at the pile side. In addition, the lateral displacement of an ungrouted pile is greater than that of a grouted pile under the same lateral load of the pile head. This indicates that a grouted pile has a good effect on controlling the lateral displacement of a single pile and can improve the elastic workspace of the pile–soil system; therefore, the lateral bearing performance and deformation control of grouted pile are significantly better than those of ungrouted pile.

Based on the determination method for the ultimate bearing capacity in the horizontal direction and the critical load of a single pile in the horizontal direction provided by the Chinese standard (JGJ 106–2014), the relationship curves of the lateral load–displacement gradients of ungrouted and grouted piles are shown in Fig. 8 to demonstrate the relationship between the lateral load and the lateral displacement during the test.

Figure 8 shows that the lateral load of the pile head corresponding to the first displacement gradient is the critical load in the horizontal direction of a single pile, while the lateral load of the pile head corresponding to the second displacement gradient is the ultimate load in the horizontal direction of a single pile. That is, the critical load in the horizontal direction of grouted pile MP2 is 320 N, and its ultimate load in the horizontal direction is 400 N. While there is no second displacement gradient in the $H-\Delta Y_0/\Delta H$ curve of the ungrouted pile, the maximum load value in the horizontal direction is taken as the ultimate load in the horizontal direction. Table 2 shows the critical load in the horizontal direction, ultimate load in the

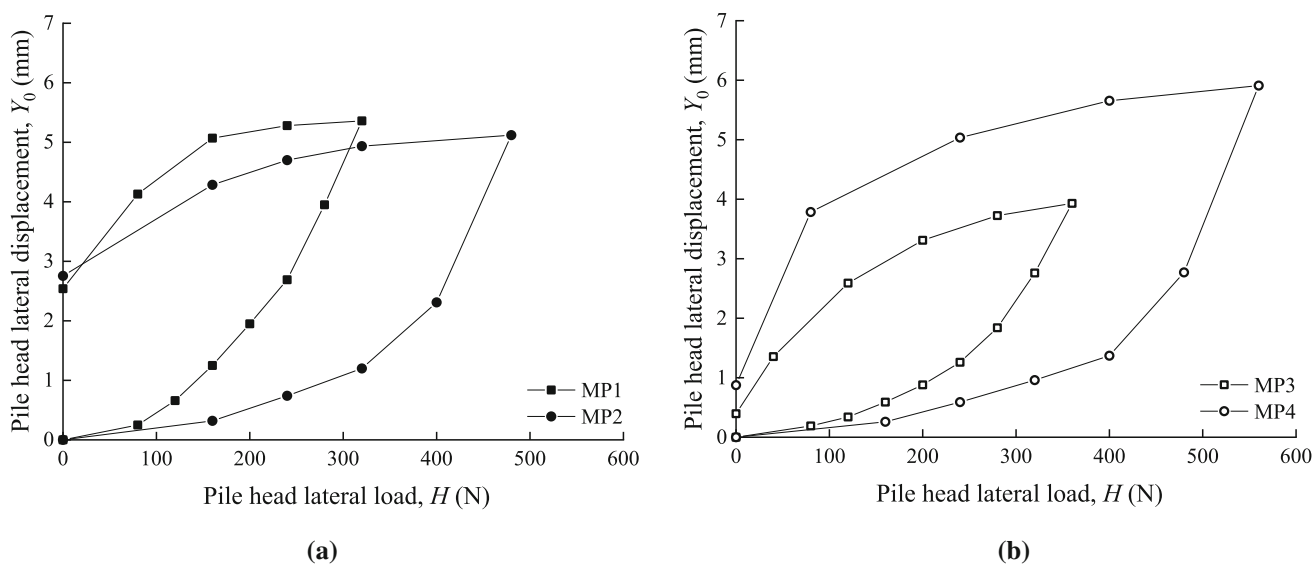


Fig. 7 Lateral load–displacement curves of piles: a calcareous sand and b siliceous sand

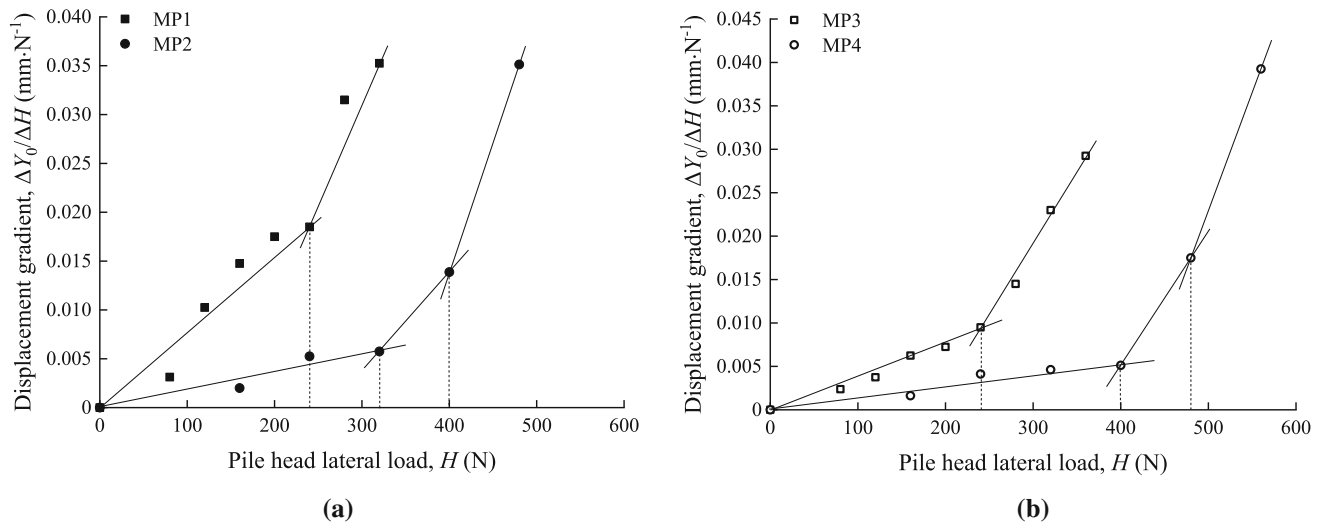


Fig. 8 Lateral load–displacement gradient curves of the piles: **a** calcareous sand and **b** siliceous sand

Table 2 Critical load, ultimate load and the increased range of each single pile

Pile no	Critical load	Displacement (mm)	Ultimate load	Displacement (mm)	H_{cr} increased range (%)	H_u increased range (%)
	H_{cr} (N)		H_u (N)			
MP1	240	2.69	320	5.36	N/A	N/A
MP2	320	1.20	400	2.31	33.33	25.00
MP3	240	1.26	360	3.93	N/A	N/A
MP4	400	1.37	480	2.77	66.67	33.33

horizontal direction and the increased range of each single pile. Table 2 shows that the lateral displacements corresponding to the critical load and ultimate load of ungrouted pile MP1 in calcareous sand are larger than those of ungrouted pile MP4 in siliceous sand. This may explain why the particularity of calcareous sand, such as brittle and fragile characteristics, causes the horizontal restraint ability of a single pile to be weaker than that of siliceous sand. In addition, compared with ungrouted piles, the critical load in the horizontal direction and ultimate load of grouted piles in calcareous sand increase by 33.33% and 25%, respectively, which indicates that postside grouting can effectively improve the horizontal bearing capacity and lateral deformation of piles in calcareous sand.

4.2 Ratio of lateral resistance coefficient of foundation soil

The ratio of the lateral resistance coefficient of foundation soil is an important design parameter of laterally loaded piles. According to the Chinese standard (JGJ 3363–2019) [27], the ratio of the lateral resistance coefficient of foundation soil for a single pile can be calculated as

$$m = \frac{(v_y H)^{\frac{5}{3}}}{b_0 Y_0^{\frac{5}{3}} (E_m I_m)^{\frac{2}{3}}} \quad (1)$$

where v_y is the lateral displacement coefficient of the pile head, which is taken as 2.441 in this test; b_0 is the calculated width of the pile, and for the circular pile, $D \leq 1$ m, $b_0 = 0.9(1.5D + 0.5)$; and $E_m I_m$ is the bending stiffness of the pile, where I_m is the moment of inertia of the pile section.

The ratio of the lateral resistance coefficient of the foundation soil for a single pile can be obtained by substituting the measured lateral load and lateral displacement of the pile head into Eq. (1) and using the bending stiffness of the pile shaft. Figure 9 shows the relationship between the m value and lateral displacement of the pile head. Figure 9 shows that m is not a certain value when the horizontally loaded pile produces lateral displacement, and the value of m exhibits a nonlinear relationship with the lateral displacement. When the lateral displacement is small, the value of m is relatively large, and the value of m changes more with decreasing the displacement. With the increase in the lateral displacement, the value of m gradually decreases and tends to be gentle. In fact, the

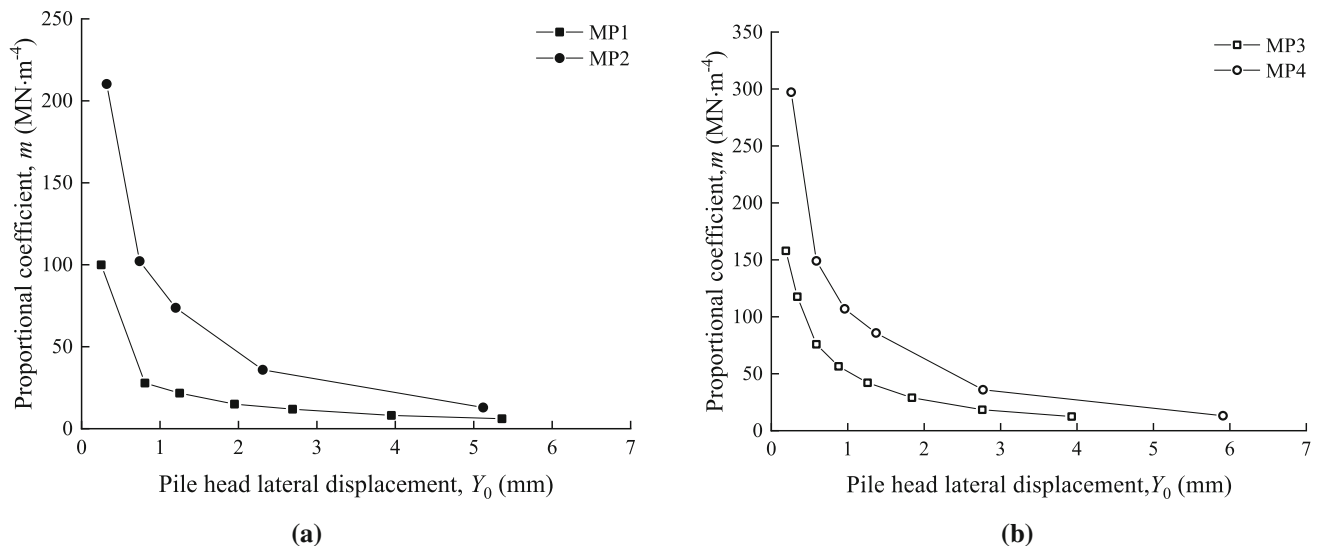


Fig. 9 Lateral displacement–proportional coefficient curves of the piles: **a** calcareous sand and **b** siliceous sand

relationship between the value of m and the lateral displacement of the pile head also reflects the nonlinear characteristics of the soil to some extent. The values of m for the ungrouted single pile in calcareous sand and siliceous sand under the ultimate load are 6.09 MN/m^4 and 12.43 MN/m^4 , respectively. The Chinese standard [27] gives the value of m of a sandy soil foundation as a range of $10\text{--}20 \text{ MN/m}^4$, indicating that the value of m of a siliceous sand foundation conforms to the recommended range given by the standard, and the value of m of the calcareous sand is less than the recommended value given by the standard due to its particularity.

Figure 9 also shows that postside grouting can improve the ratio of the lateral resistance coefficient of foundation soil, which is related to the solidification of cement grout, which improves the strength of soil and increases the elastic modulus of soil. In addition, there is a nonlinear relationship between the value of m and the horizontal force of the pile head. The value of m is higher under a lower load level; with the increase in the load level, plastic deformation of the soil around the pile occurs, and the value of m gradually decreases. Therefore, the value of m is affected by the lateral displacement of the pile head, soil properties and load level, and the lateral displacement and soil properties around the pile are the key factors that affect the value of m .

4.3 Bending moment of a single pile

The bending deformation of a single pile under horizontal loading is mainly affected by the soil properties, pile diameter and piling quality. The bending moment distribution of a single pile under different lateral loads can be calculated based on the data collected by strain gauges

arranged on each section of the pile. According to the relevant analysis theory in material mechanics, the bending moment M on any pile section can be calculated by the following formula:

$$M = \frac{E_m I_m \Delta \varepsilon}{s_0} \quad (2)$$

where $\Delta \varepsilon$ is the strain difference measured by the two symmetrical strain gauges on the section of the pile and s_0 is the spacing between the two symmetrical strain gauges arranged on the section of the pile.

Figure 10 shows the curve of the bending moment along the depth under different levels of loading. Figure 10 shows that the bending moment of a single pile increases first and then decreases with increasing pile depth, and the bending moment of a single pile increases uniformly with increasing lateral load. After reaching the critical load of a single pile, the bending moment of the pile shaft increases greatly, and the soil around the pile enters the elastic–plastic stage. The positions of the maximum bending moments of the ungrouted pile and grouted pile are approximately the same, which occur at approximately 0.1 m ($5D$) below the surface of the model foundation. This depth is the main influencing depth of the bending moment of the pile shaft. As the horizontal load increases, the bending moment of the pile shaft gradually develops toward the deep soil layer, so that the middle and lower soil layers also bear the horizontal load. During the entire test loading process, the bending moment of a single pile is mainly distributed in the range above 0.3 m and tends to zero after exceeding this range. In addition, comparing the performance of ungrouted piles and grouted piles, it is evident that grouted piles have a greater resistance to the bending moment of the pile foundation by improving the

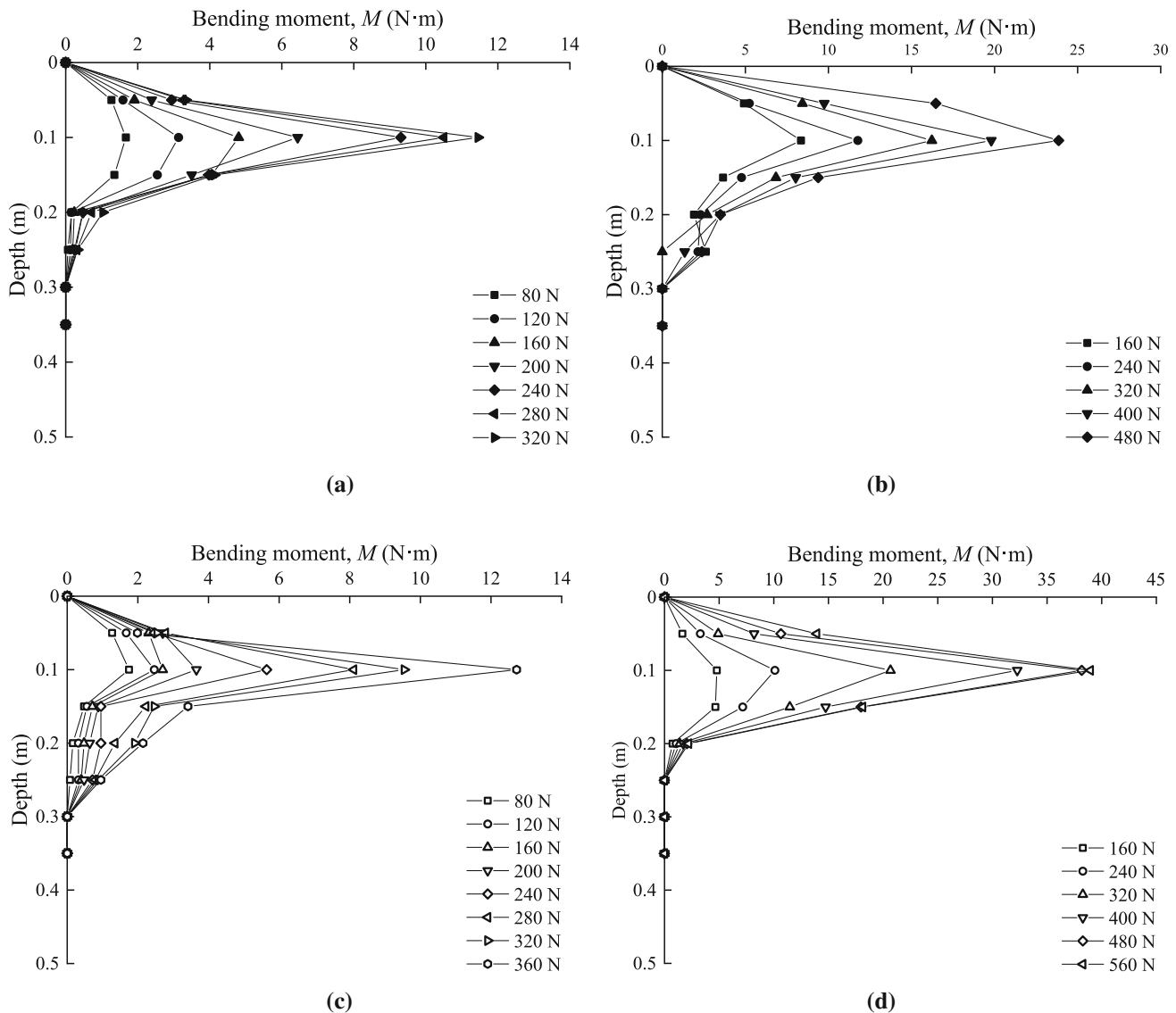


Fig. 10 Bending moment of the pile shaft at different levels of loading: **a** MP1; **b** MP2; **c** MP3; and **d** MP4

physical and mechanical properties of the upper soil layer, thereby effectively improving the horizontal bearing performance of the pile foundation.

4.4 Lateral displacement of a pile shaft

The deflection of the pile can be directly obtained by the double integration of the bending moment, which can be calculated as follows:

$$y = \iint \frac{M}{E_m I_m} dz^2 \tag{3}$$

where y is the lateral displacement of the section of the pile and z is the embedding depth of the strain gauge.

According to Eq. (3), the lateral displacement of the pile shaft can be indirectly calculated from the bending moment of the pile shaft. The distribution curve of the lateral displacement of the pile shaft under different levels of loading is shown in Fig. 11. As shown in Fig. 11, the lateral displacement of the pile shaft shows obvious nonlinear characteristics with increasing depth and exhibits a decreasing trend. The lateral displacement of the pile shaft increases gradually with increasing horizontal load, and the lateral displacement increases greatly after the load reaches a certain value, showing strong nonlinear characteristics. When the pile depth exceeds 0.2 m, the lateral displacement is close to 0, indicating that the lateral load of the pile head has a small or negligible effect on the lateral

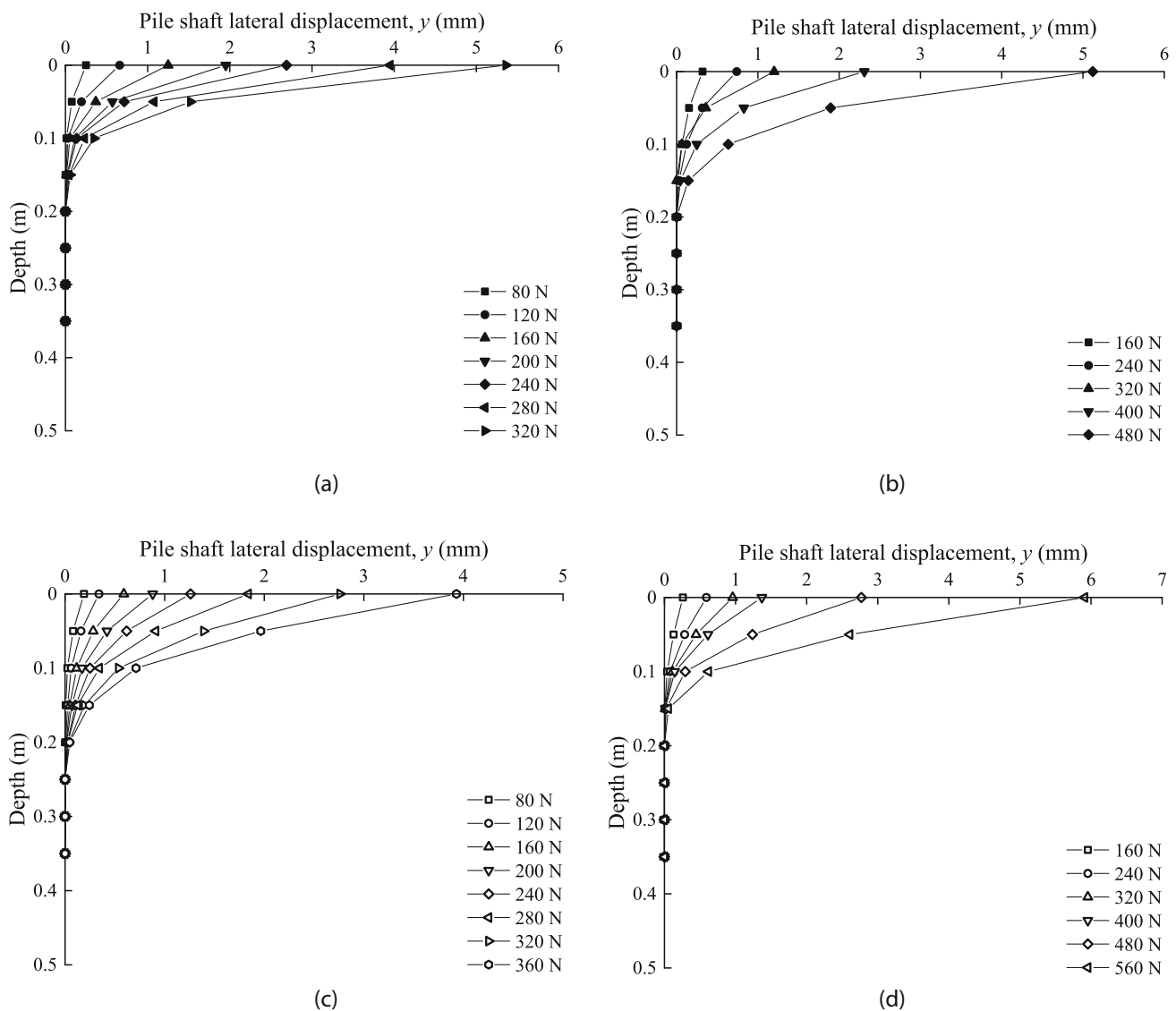


Fig. 11 Lateral displacement of the pile shaft at different levels of loading: **a** MP1; **b** MP2; **c** MP3; and **d** MP4

displacement of the lower pile. In addition, the lateral displacement of the pile shaft decreases to some extent after side grouting. The corresponding lateral displacements of the ungrouted piles MP1 and MP3 under the ultimate load are 5.36 mm and 3.93 mm, respectively, and the corresponding lateral displacements of the grouted piles MP2 and MP4 under the above-mentioned corresponding loads are 1.20 mm and 1.17 mm, respectively. Compared with the lateral displacement of ungrouted piles, the lateral displacements of grouted piles are reduced by 77.61% and 70.23%, respectively. This shows that the injected grout can strengthen the soil around the pile and improve the strength of the soil, and the cement grout has a significant effect on improving the calcareous sand formation; therefore, the single pile can effectively resist the lateral deformation under horizontal loading and exhibits

characteristics that are roughly the same as those of a pile in siliceous sand after grouting.

4.5 Lateral soil resistance

The earth pressure on the side of the pile is caused by the bending moment deformation of the pile, which is the result of the pile–soil interaction. According to the miniature FBG earth pressure cells labeled F1 to F5 embedded around the pile, the variation law of the soil resistance when a single pile is horizontally loaded can be obtained, while the variation of the soil resistance measured by the miniature FBG earth pressure cells labeled F6 to F9 is small, which is not discussed here. The variation curves of the lateral soil resistance measured by the miniature earth

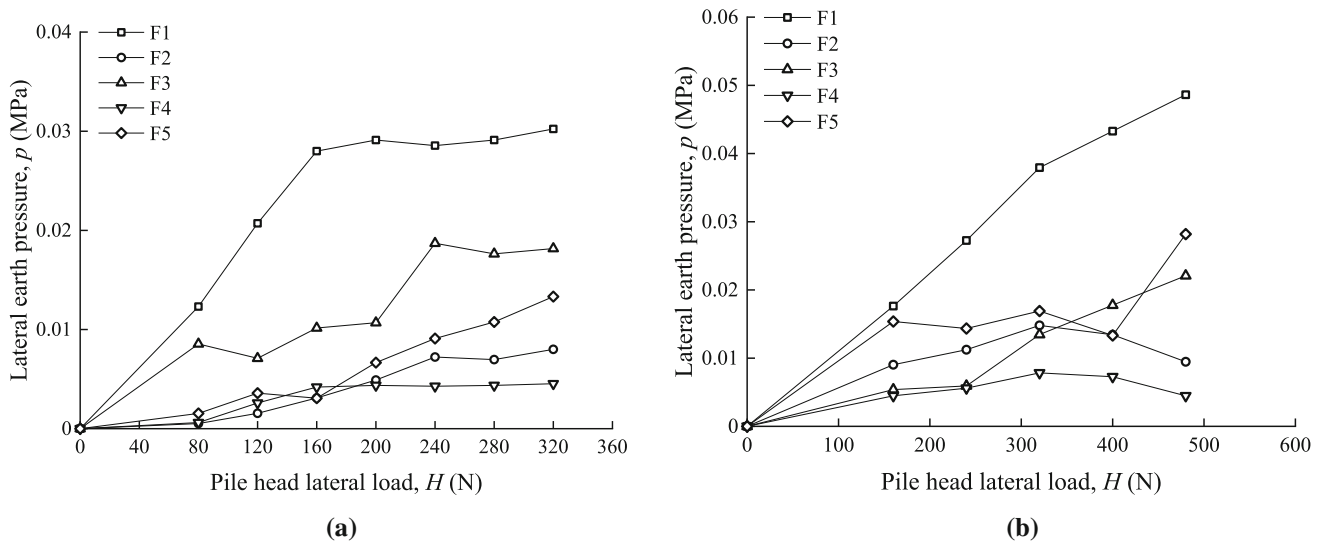


Fig. 12 Lateral load–soil reaction curves of piles in calcareous sand: **a** MP1 and **b** MP2

pressure cells labeled F1 to F5 with the lateral load on the pile head are shown in Fig. 12.

It can be seen from Fig. 12 that the lateral soil reaction gradually increases with the increase in the lateral load on the pile head, and when the lateral load is constant, the lateral soil reaction measured by the miniature earth pressure cells labeled F1, F3 and F5 decreases along the increase in the pile depth. That is to say, the lateral soil reaction in the upper part of the shallow layer is large, while the lateral soil reaction in the lower part of the pile is small. Hence, the lateral resistance of the pile side is mainly controlled by the physical and mechanical indexes of the soil in the upper part of the shallow layer. The measured soil resistance changes of the miniature earth pressure cells labeled F2 and F4 embedded in the inner side of the model container are small, and the values are about 5 kPa. When the horizontal load is large, some of the values are less than 10 kPa. This indicates that when the distance between the model pile and the inner side of the model container exceeds $8.5D$, the force generated by the lateral loaded pile on the boundary is small or the influence of the boundary effect on the test results can be ignored. In addition, the variation of the soil resistance of the upper part of the grouted pile is more obvious than that of the ungrouted pile; that is, the maximum soil resistance increases under the condition of a large lateral load, which is due to the injected cement grout enhances the strength of the soil around the pile, so that it can provide a higher lateral soil resistance.

5 Grout distribution and microstructure analysis of post-grouted single piles

5.1 Penetration and diffusion of grout after single-pile excavation

To observe the penetration and diffusion of the injected grout in the model foundation, the sand samples in the model container were excavated after the horizontal static load test was completed. The cement-stabilized soil was removed, and its size was measured. The diffusion range of the cement grout in the sand samples of the model foundation was analyzed. The cement-stabilized soil removed with the grouted pile is shown in Fig. 13. Figure 13 shows that the cement grout of the grouted pile moves upward along the pile shaft and forms a “flange body” with a large thickness. The grout migration height is approximately 6–8 cm (approximately $3D$ – $4D$, where D is the pile diameter), and the thickness of the grout on the pile shaft is approximately 2–6 mm. In addition, the figure shows that the lateral diffusion distance of cement grout in calcareous sand can reach $7.5D$ away from the pile side, the lateral diffusion distance of cement grout in siliceous sand can also reach $8.5D$ away from the pile side, and an irregular “flange body” with a different thickness is formed. The cement grout injected at the pile side moves upward along the pile shaft and spreads horizontally, forming a stable structure of cement-stabilized soil with the sand sample of the model foundation, so that the pile–soil system interaction enters a new structural equilibrium state.

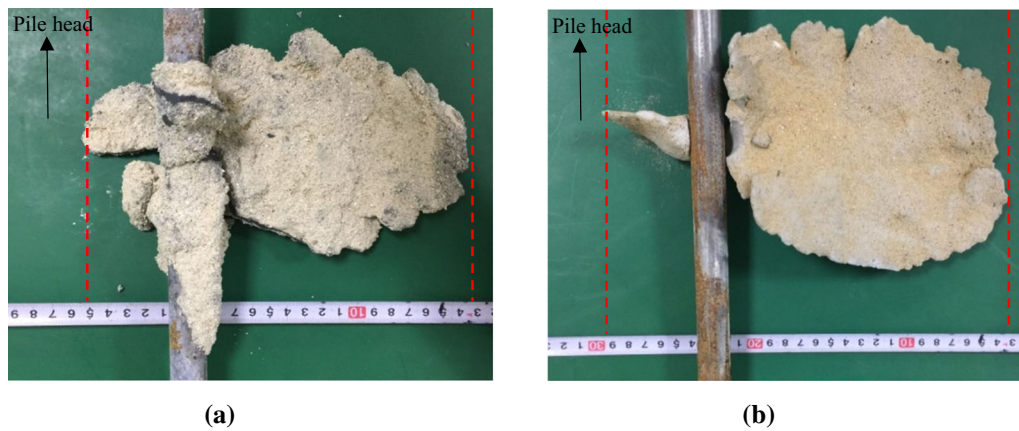


Fig. 13 Cement-stabilized soil for a single pile with grouting: **a** calcareous sand and **b** siliceous sand

5.2 Microstructure analysis of cement-stabilized soil

Scanning electron microscopy (SEM) was used to analyze the change of microstructure of calcareous sand cement-stabilized soil. SEM observation is the most direct and effective means to study the microstructure morphology of cement-stabilized soil. To ensure that the microstructure image obtained by scanning can reflect the real state of the sample, the undisturbed sample should be selected to be as close to the test sample as possible to maintain the original state of the soil and exhibit good conductivity. In this experiment, representative block samples are selected to prepare SEM microscopic samples. The preparation steps of the test samples are as follows: (1) drying the samples. The sliced block samples were placed in a low-temperature vacuum dryer and dried at a low temperature (below 40 °C) for 24 h. (2) Making the samples. After drying, the samples were broken to obtain undisturbed samples with a size of approximately 10 × 10 mm and a thickness of 2–4 mm, and the observation surface was as smooth as possible. (3) Gold spraying coating. To enhance the conductivity of the observed sample, a gold film was sprayed

on the surface of the sample before observation. Before putting the sample into the ion sputtering instrument, the particles floating on the surface of the sample were blown out by a bulb syringe to complete the coating.

Before testing the cement-stabilized soil sample, unreinforced calcareous sand and siliceous sand were first observed by SEM. Figure 14 shows the SEM images of the original calcareous sand and siliceous sand. Figure 14 shows that the structural morphology of undisturbed calcareous sand and siliceous sand is granular in the low-multiple image. The particle shape of calcareous sand is significantly different from that of siliceous sand. The particle shape of calcareous sand is polygonal and sharp, while the edges of siliceous sand are relatively smooth. In the high-resolution image, the surface of siliceous sand particles is relatively flat, while the surface of calcareous sand particles is rough and uneven, and there are more pores. The morphological characteristics of unreinforced siliceous sand and calcareous sand are quite different, which leads to differences in the engineering characteristics of the two.

Figure 15 shows SEM images of calcareous sand and siliceous sand of the cement-stabilized soil samples. In

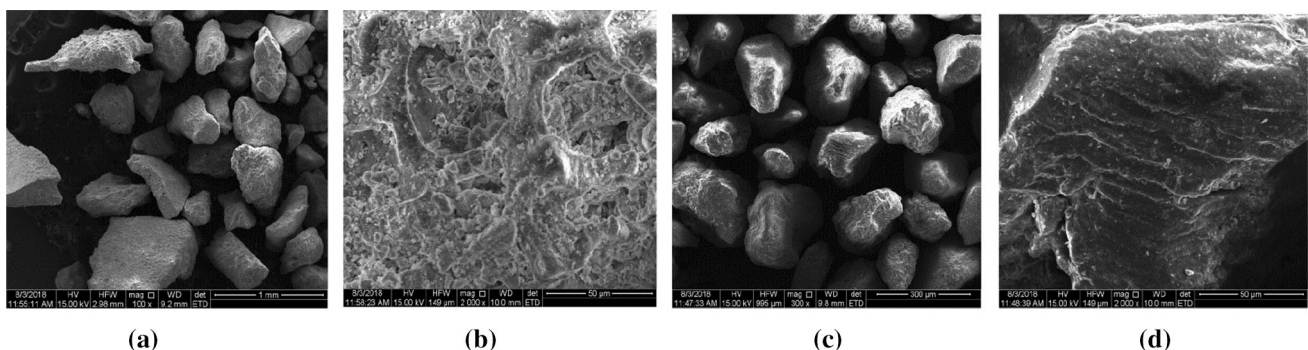


Fig. 14 SEM images of the original sand samples: **a** calcareous sand × 100; **b** calcareous sand × 2000; **c** siliceous sand × 300; and **d** siliceous sand × 2000

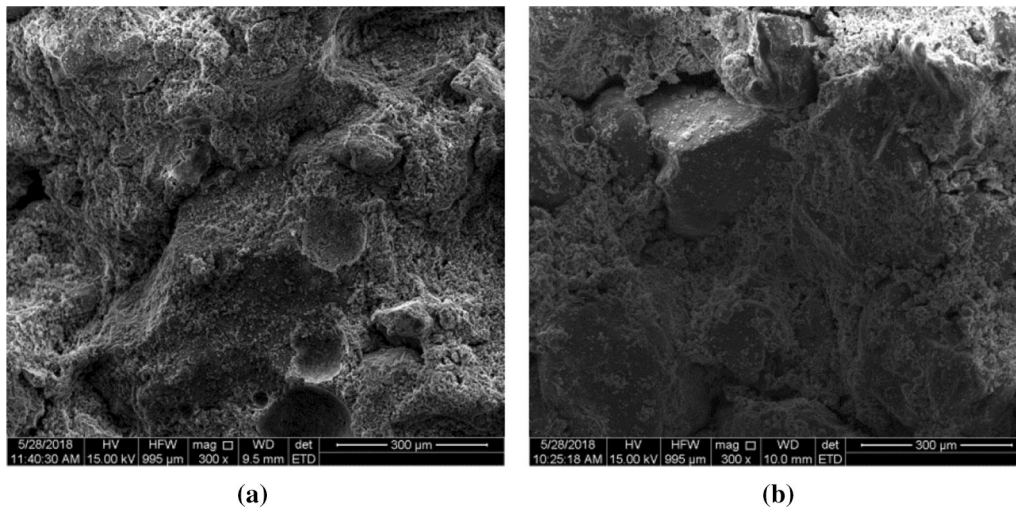


Fig. 15 SEM images of cement-stabilized soil samples: **a** calcareous sand and **b** siliceous sand

Fig. 15, it is evident that compared with performance of the sand sample before grouting, the sand sample after grouting improves the adhesion between particles due to the incorporation of cement, which improves the integrity of the cement-stabilized soil to varying degrees, thereby increasing the strength of cement-stabilized soil. This is mainly because the cement hydration products are connected to each other and fill the pores between the sand particles, which makes it difficult to differentiate the morphology of the sand particles, cement and hydration products; therefore, the sand particles, cement, hydration products connect to form a whole system with high strength. There is a large difference in the particle morphology between the unreinforced calcareous sand and the siliceous sand, while the reinforced calcareous sand and the siliceous sand form a dense massive structure. Therefore, the post-grouting technique can achieve better results for the reinforcement of the pile foundation in siliceous sand and calcareous sand compared to that of piles without post-grouting. This conclusion further confirms the results of the static load test.

6 Discussion

The test results have demonstrated that postside-grouting technique can improve the lateral bearing performance and deformation control ability of pile in calcareous sand by enhancing the strength of the upper soil around the pile, and it has roughly the same effect on improving the bearing performance of pile in calcareous sand and siliceous sand. The results are consistent with the conclusions reported by Wan et al. [36] that the strength variation of cement-stabilized soil of calcareous sand and siliceous sand under seawater erosion environment have similar characteristics.

In addition, through the analysis of bending moment, lateral displacement of the pile shaft and soil resistance distribution in calcareous sand stratum, it can be found that improving the physical and mechanical properties of the upper soil layer can effectively improve the ability of pile to resist lateral load and can more effectively control the lateral displacement of the pile shaft and provide higher soil resistance. This conclusion is consistent with the results obtained in the existing literature [24].

As the bearing capacity of super-long friction pile or horizontal loaded pile depends mainly on the side friction of the upper part of the pile or the soil resistance of the upper part of the pile side, it is more critical to enhance the side resistance or the soil resistance, so more attention should be paid to the adhesion between the entire pile and the soil. The static load test and excavation observation analysis show that the upper soil has a greater influence on the lateral bearing capacity of the pile, and the uncertainty of the flow direction of the cement grout injected during the grouting process makes it unevenly distributed along the pile shaft and formed an irregular cement-stabilized mass, resulting in that the grout cannot effectively cover the side surface of the pile, and the pile–soil system fails to form a closely coordinated system. To solve the problem of the uncertainty of the flow direction of the grout and the inability to form an ideal geometric grout bubble, some scholars [19, 25, 28] developed an ideal geometric grout bubble device after grouting of prefabricated piles and cast-in-place piles, which the grouting amount and grouting pressure can be effectively controlled to form an ideal geometric grout bubble. The increase range of side and base resistances can be calculated according to the ideal geometric grout bubble size, so that the post-grouting technique is more reasonable. At the same time, to solve the problems of large section spacing, low plugging rate of

grouting holes and uneven grout distribution of the existing post-grouting device at the pile side, the authors first proposed the concept of distributed post-grouting for super-long piles and developed a set of distributed post-grouting device. The main technical features of the device are as follows: the grouting outlet is preset at a certain distance each interval of the grouting pipe, and the grouting pipe is fixed on the pile shaft before the pile is formed. During the grouting, the grouting core tube is lowered to the designated location of the grouting outlet by lifting the positioning device. The high-pressure rubber in the stop-grouting plug is expanded by air pressure to form a sealing space with the grouting pipe, and then, the grouting core tube is grouted to achieve the effect of layered grouting. After the grouting of the same section is finished, the grouting core tube is moved to the next preset location of the grouting outlet by lifting the positioning device until the side grouting is completed. The distributed post-grouting device can effectively cover the outer surface of the pile with the injected grout and realize the effective bonding and load transfer between the pile shaft and the sediment, thus expanding the application prospect of the pile foundation in calcareous sand. Therefore, it is suggested to adopt directional post-grouting device or distributed post-grouting device in future practical projects to reduce the uncertainties in the post-grouting process, so that the injected cement grout can effectively cover the pile shaft and form a new structural equilibrium state, so as to ensure the expected effect of post-grouting.

7 Conclusions

This paper presents a model static load test of ungrouted piles and postside-grouted piles in calcareous sand to study the response of postside-grouted piles subjected to lateral loading and compares the obtained results to the test results of ungrouted piles and postside-grouted piles in siliceous sand. The distribution and microstructure of cement-stabilized soil are analyzed through the excavation of a post-grouting single pile. The following conclusions can be drawn according to the test results and analyses.

1. The change in the lateral displacement of the pile head with the lateral force of the pile head in calcareous sand is different from that in siliceous sand due to the particularity of the calcareous sand, and the horizontal restraint ability of a single pile without grouting in calcareous sand is weaker than that in siliceous sand. Compared with the lateral bearing capacity of an ungrouted pile, the lateral bearing capacity of a post-grouted pile in calcareous sand is greatly improved, and the lateral displacement of the post-grouted pile head decreases by more than 70% under the same conditions. This indicates that the

postside-grouted pile can effectively improve the lateral bearing capacity of the pile foundation in calcareous sand and can greatly enhance the deformation control ability of the pile foundation.

2. The ratio of the lateral resistance coefficient of calcareous sand is less than the recommended value given by the specification due to its particularity, the strength of the soil around the pile is enhanced by the solidification of the injected grout, and the ratio of the lateral resistance coefficient of the soil around the pile increases. The ratio of the lateral resistance coefficient of ungrouted and post-grouted piles gradually tends to be consistent with the increase in the lateral displacement of the pile head.

3. The maximum bending moments of the post-grouted and ungrouted piles are located at a depth of $5D$ below the loading surface, which is the main influencing depth of the bending moment. Lateral deformation mainly occurs in the upper part of the pile shaft under lateral loading, and the influence on the lower part of the pile shaft can be ignored. Grouting can effectively enhance the ability of pile foundations to resist horizontal loads and control deformation by improving the physical and mechanical properties of the upper soil layer.

4. The cement grout injected into the pile side moves upward, infiltrates downward and diffuses laterally along the pile shaft, filling the uneven holes on the surface of calcareous sand and forming a stable structure of cement-stabilized soil, enhancing the interface meshing between calcareous sand particles and cement grout. Therefore, the pile–soil system interaction enters a new structural equilibrium state, which effectively improves the physical and mechanical properties and interface structure performance of the undisturbed soil around the pile, and improves the horizontal bearing performance of pile foundations in calcareous sand to a certain extent.

Acknowledgements This work was supported by the National Natural Science Foundation of China (52008100; 51878160) and Natural Science Foundation of Jiangsu Province (BK20200400).

References

1. Agarwal SL, Malhotra AK, Banerjee R (1977) Engineering properties of calcareous soils affecting the design of deep penetration piles for offshore structures. Proceedings of the 9th Annual Offshore Technology Conference, Houston
2. Angemeer J, Carlson ED, Klick JH (1973) Techniques and results of offshore pile load testing in calcareous soils. Proceedings of the 5th Annual Offshore Technology Conference, Houston, pp 677–692
3. Angermeier J, Carlson E, Stroud S, Kurzeme M (1975) Pile load tests in calcareous soils conducted in 400 feet of water from a semi-submersible exploratory rig. Proceedings of 7th Annual Offshore Technology Conference, Houston

4. Bruce DA (1986) Enhancing the performance of large diameter piles by grouting. *Ground Eng* 19(4):9–15
5. Byrne GP, Strydom JH, Du Preez W (1999) The performance of piled foundations supporting a large hotel on estuarine deposits in Durban. 7th International Conference and Exhibition on Piling and Deep Foundations, Vienna
6. Chen JW (2013) Application of cast-in-site bored pile in coral rock. *Resour Environ Eng* 27(6):769–772 ((in Chinese))
7. Craig WH (1984) Installation studies for model piles. Proceedings of symposium on the application of centrifuge modeling to geotechnical design, Manchester, pp 440–455
8. Dai GL, Gong WM, Zhao XL, Zhou XQ (2010) Static testing of pile-base post-grouting piles of the Suramadu bridge. *Geotech Test J* 34(1):34–49
9. Dai GL, Wan ZH, Zhu MX, Gong WM (2018) The model of grout migration height for pressured grouting at the pile tip based on time-dependent behavior of viscosity and its application. *Rock Soil Mech* 39(8):2941–2950 ((in Chinese))
10. Datta M, Gulhati SK, Rao GV (1980) An appraisal of the existing practice of determining the axial load capacity of deep penetration piles in calcareous sands. Proceedings of the 12th Annual Offshore Technology Conference, Houston
11. Dutt RN, Cheng AP (1984) Frictional response of piles in calcareous deposits. Proceedings of the 16th Annual Offshore Technology Conference. Houston, pp 527–530
12. Ghazali FM, Sotiropoulos E, Mansour OA (1988) Large-diameter bored and grouted piles in marine sediments of the Red Sea. *Can Geotech J* 25(4):826–831
13. Gilchrist JM (1985) Load tests on tubular piles in coralline strata. *J Geotech Geoenviron Eng* 111(5):641–655
14. Gouvenot D, Gabaix JC (1975) A new foundation technique using piles sealed by cement grout under high pressure. Offshore Technology Conference, pp 645–656.
15. Joer HA, Randolph MF, Gunasena U (1998) Experimental modeling of the shaft capacity of grouted driven piles. *Geotech Test J* 21(3):159–168
16. Littlechild BD, Plumbridge GD, Free M W (1998) Shaft grouted piles in sand and clay in Bangkok. Proc. 7th International Conference and Exhibition on Piling and Deep Foundations, pp 171–178
17. Liu XC, Xu J, You XP, Xie F (2019) Study on bearing behavior of large diameter driven steel pipe pile in coral reef geology. *The Ocean Eng* 37(6):157–163 ((in Chinese))
18. McClelland B (1974) Design of deep penetration piles for ocean structures. *J Geotech Geoenviron Eng* 100(7):709–747
19. Mullins G, Dapp S, Frederick E, Wanger V (2001) Post grouting drilled shaft tips: phase I. Research report University of South Florida, Tampa, USA, pp 127–156
20. McVay M, Thiyyakkandi S, Joiner J, Adams V (2010) Group efficiencies of grout-tipped drilled shafts and jet-grouted piles. University of Florida, Gainesville
21. Nauroy JF, Le Tirant P (1985) Driven piles and drilled and grouted piles in calcareous sands. Proceedings of the 17th Annual Offshore Technology Conference. Houston, pp 83–91
22. Ovesen NK (1979) The use of physical models in design: the scaling law relationships. Proceedings of 7th European conference on soil mechanics and foundation engineering, Brighton, 4: 318–323
23. Robson RJ, Wahby A (1994) Base and shaft grouted bored pile foundations for the first residential complex. Proceedings of the International Conference on Piling and Deep Foundations. Rotterdam
24. Rollins KM, Adsero ME, Dan AB (2009) Jet grouting to increase lateral resistance of pile group in soft clay. Proceedings of International Foundation Congress and Equipment Expo. Orlando, pp 265–272
25. Schwartz LJ III (2012) Demonstrating the ability to develop cylindrical and spherical cavity expansions on drilled shafts in cohesionless soils through full scale experimentation. M.S. thesis, University of Florida, Gainesville
26. The Professional Standards Compilation Group of People's Republic of China (2014). Technical code for testing of building foundation piles. JGJ 106–2014. China Architecture & Building Press, Beijing (in Chinese))
27. The Professional Standards Compilation Group of People's Republic of China (2019) Code for design of ground base and foundation of highway bridges and culverts. JTJ3363–2019. China Communications Press, Beijing (in Chinese)
28. Thiyyakkandi S (2013) Study of grouted deep foundations in cohesionless soils. PH.D. thesis, University of Florida, Gainesville.
29. Thiyyakkandi S, McVay M, Bloomquist D, Lai P (2013) Measured and predicted response of a new jetted and grouted precast pile with membranes in cohesionless soils. *J Geotech Geoenviron Eng* 139(8):1334–1345
30. Thiyyakkandi S, McVay M, Bloomquist D, Lai P (2014) Experimental study, numerical modeling of and axial prediction approach to base grouted drilled shafts in cohesionless soils. *Acta Geotech* 9(3):439–454
31. Wan ZH, Dai GL, Gong WM (2017) Post-grouting of drilled shaft tips in coral-reef limestone formations: a case study. In: Proceedings of the 27th international ocean and polar engineering conference, San Francisco, USA, pp 719–724
32. Wan ZH, Dai GL, Gong WM (2018) Full-scale load testing of two large-diameter drilled shafts in coral-reef limestone formations. *Bull Eng Geol Environ* 77(3):1127–1143
33. Wan ZH, Dai GL, Gong WM (2018) Enhanced mechanism of post-grouting pile in coral-reef limestone formations. *Rock and Soil Mech* 39(2):467–473 ((in Chinese))
34. Wan ZH, Dai GL, Gong WM (2019) Field study on post-grouting effects of cast-in-place bored piles in extra-thick fine sand layer. *Acta Geotech* 14(5):1357–1377
35. Wan ZH, Dai GL, Gong WM (2020) Field and theoretical analysis of the response of axially loaded grouted drilled shaft in extra-thick fine sand. *Can Geotech J* 57(3):391–407
36. Wan ZH, Dai GL, Gong WM, Gao LC (2021) Experimental study on micro-erosion mechanism of cement stabilized calcareous sand under seawater environment. *Rock and Soil Mech* 42(7):1871–1882 ((in Chinese))
37. Wees JA, Chamberlin RS (1971) Khazzan Dubai No 1 Pile design and installation. *J Geotech Geoenviron Eng* 97(10):1415–1429
38. Zhou JJ, Gong XN, Wang KH, Zhang RH (2018) Shaft capacity of the pre-bored grouted planted pile in dense sand. *Acta Geotech* 13(5):1227–1239
39. Zhou JJ, Gong XN, Zhang RH, Naggar MHE, Wang KH (2020) Field behavior of pre-bored grouted planted nodular pile embedded in deep clayey soil. *Acta Geotech* 15(9):1847–1857
40. Zhou JJ, Yu JL, Gong XN, Naggar MHE, Zhang RH (2021) Field study on the behavior of pre-bored grouted planted pile with enlarged grout base. *Acta Geotech*. <https://doi.org/10.1007/s11440-021-01208-7>